Optimal Fault-Tolerant Path-Tracking Control for 4WS4WD Electric Vehicles

Hao Yang, Vincent Cocquempot, and Bin Jiang

***Abstract*—This paper investigates the path-tracking problem for four-wheel-steering and four-wheel-driving electric vehicles with input constraints, actuator faults, and external resistance. A hybrid fault-tolerant control approach, which combines the linear-quadratic control method and the control Lyapunov function technique, is proposed. It not only maintains the vehicle's tracking performance in spite of faults, input constraints, and external resistance but also reduces the cost of the fault-tolerant process. A prototype vehicle from the Laboratoire d'Automatique, Génie Informatique et Signal (LAGIS), is particularly focused on illustrating the applicability of our approach.**

***Index Terms*—Bounded hybrid control, electric vehicles (EVs), fault-tolerant control (FTC), path tracking.**

I. Introduction

Electric vehicles (EVs) have attracted a great deal of interest as a powerful solution to environmental and energy problems [1], [2]. The four-wheel steering and four-wheel-driving (4WS4WD) EV not only takes the advantage of a four-wheel-driving vehicle where the individual torque of each wheel can be independently controlled [3] but also benefits from the four-wheel steering structure where both the steering positions of front wheels and rear wheels can be controlled [4]. The 4WS4WD EVs have two big advantages over conventional cars. First, electric motors can be controlled much more precisely, with a much shorter control period. This leads to a more effective antiskid braking system or traction control system. Second, there exist four in-wheel motors; the torque of each drive wheel can be controlled. Such structure significantly improves the EV's lateral dynamics, particularly for the situation of path tracking [4], [5].

Faults may lead to a vehicle's abnormal behaviors. The faults that mainly degrade the vehicle's performance include faults of sensors that provide important physical characteristics (e.g., the vehicle speed and the sideslip angle) and actuator faults such as the malfunction of the steering systems and wheel torque controllers. The fault detection and isolation (FDI) techniques of vehicles have been intensively investigated [6]–[10]. Fault-tolerant control (FTC) approaches of vehicles have also been developed to guarantee the safety of the vehicle [11], [12].

However, to the best of our knowledge, few contributions have been made for the fault-tolerant path-tracking control of 4WS4WD EVs. This paper is important since EVs have more complicated control structures than conventional cars, and the path tracking of EVs is also one of the key issues in an intelligent transportation system. The tracking performance must be maintained in spite of faults; otherwise, traffic accidents may occur, which may lead to the vehicle's destruction. Moreover, most of the related FTC works do not address the issues of optimality, input constraints, and external resistance.

1) Optimality reduces a cost function of the states and inputs of the vehicle systems as much as possible, which is needed for FTC.
2) Input constraints are involved to prevent the vehicles from skidding or spinning when FTC is activated.
3) External resistance includes the air resistance, wind effects, the deformation of the wheels, and the internal friction of the vehicle. These factors always affect the vehicle.

In this paper, we focus on the optimal fault-tolerant path-tracking control for a 4WS4WD EV in the Laboratoire d'Automatique, Génie Informatique et Signal (LAGIS). This prototype vehicle, which is named RobuCar, is built by the Robosoft Company [13]. Several important types of actuator faults are considered. A hybrid control approach is proposed, which combines the linear-quadratic (LQ)-based progressive accommodation (PA) method [14] and the control Lyapunov function (CLF) technique [16]. The motivation for developing such a control structure is to maintain the vehicle's tracking performance in spite of faults, input constraints, and external resistance and, meanwhile, reduce the cost function of states and inputs that result from the FTC algorithm. This paper does not consider FDI techniques. For fruitful results of such FDI techniques, see [6]–[10]. The sensor faults are also not involved; some related work can be seen in [6]. The rest of this paper is organized as follows. Section II gives a brief description of the vehicle model and the considered faults. The FTC design is developed in Section III. The application to the RobuCar is discussed in Section IV, followed by some concluding remarks in Section V.

II. Preliminaries

A. Vehicle Model

The features of the RobuCar dynamics are described in Fig. 1. Our system comprises a 4WS4WD vehicle body, four wheels, and a reference path for tracking. The distance between the center of gravity (CG) and the front axle (respectively, rear axle) is l_f (respectively, l_r), and l_d is one half of the tread. r_{ei} $(i = 1, 2, 3,$ and $4)$ denotes the effective radius of the wheel i.

The state variables are the speed of the CG v, the sideslip angle β, the yaw rate γ, the perpendicular distance y_c between the vehicle and the reference path, and the angle ϕ between the vehicle and the tangent to the straight path. The traction forces f_{xi} and f_{yi} are transmitted from the road surface via the wheels to the vehicle chassis. The input variables to be applied are the steering angle δ_i and the torque T_i. As for the RobuCar, the command of the steering angle is the same for the two front (rear) wheels. Denote $\delta_f \triangleq \delta_1 = \delta_2$ and $\delta_r \triangleq \delta_3 = \delta_4$ as the steering angles of the front wheels and the rear wheels, respectively. In fact, when taking a turn, the steering angle of the inner wheel would be a little bigger than that of the outer wheel. This small modeling error is quite accepted in real situations, as in many related works [3], [5].

Manuscript received January 7, 2008; revised September 12, 2008. First published October 16, 2009; current version published March 3, 2010. This work was supported in part by International Campus on Safety and Intermodality in Transportation, by the National Natural Science Foundation of China under Grant 60874051, by the 973 Program of China under Grant 2009CB320600, and by the Graduate Innovation Research Funding of Jiangsu Province under Grant CX07B-112z. The Associate Editor for this paper was S. Darbha.

H. Yang is with College of Automation Engineering, Nanjing University of Aeronautics and Astronautics, Nanjing 210016, China, and also with the Laboratoire d'Automatique, Génie Informatique et Signal, UMR CNRS 8146, Université des Sciences et Technologies de Lille, 59655 Villeneuve d'Ascq Cedex, France (e-mail: younghao82@yahoo.com.cn).

V. Cocquempot is with the Laboratoire d'Automatique, Génie Informatique et Signal, UMR CNRS 8146, Université des Sciences et Technologies de Lille, 59655 Villeneuve d'Ascq Cedex, France (e-mail: vincent.cocquempot@univ-lille1.fr).

B. Jiang is with the College of Automation Engineering, Nanjing University of Aeronautics and Astronautics, Nanjing 210016, China (e-mail: binjiang@nuaa.edu.cn).

Color versions of one or more of the figures in this paper are available online at http://ieeexplore.ieee.org.

Digital Object Identifier 10.1109/TITS.2009.2033374

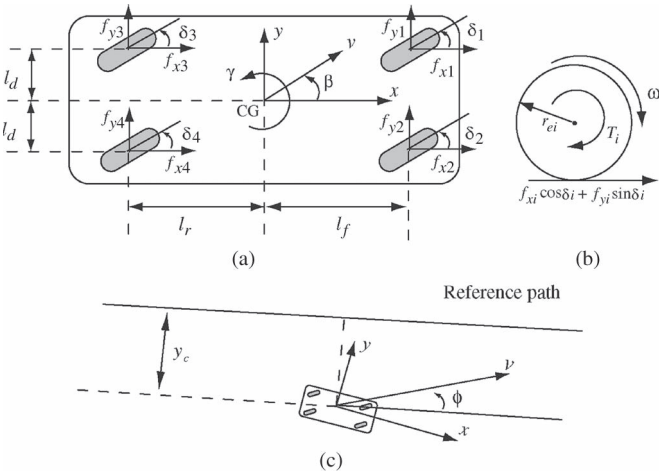

Fig. 1. Vehicle system.

We briefly give the dynamical equations of the vehicle body, wheel, and path-tracking kinematics; more details can be seen in [4], [10], and [17].

Vehicle body dynamics:

$$\begin{bmatrix} m & 0 & 0 \\ 0 & mv & 0 \\ 0 & 0 & J_z \end{bmatrix} \frac{d}{dt} \begin{bmatrix} v \\ \beta \\ \gamma \end{bmatrix} = \begin{bmatrix} \cos\beta & \sin\beta & 0 \\ -\sin\beta & \cos\beta & 0 \\ 0 & 0 & 1 \end{bmatrix} \times \sum_{j=1}^{4} \begin{bmatrix} f_{xj} \\ f_{yj} \\ M_{zj} \end{bmatrix} - \begin{bmatrix} 0 \\ mv\gamma \\ 0 \end{bmatrix} \quad (1)$$

where m denotes the mass of the vehicle. J_z is the moment of inertia. M_{zj} is the yaw moment.

Wheel dynamics:

$$I_{\omega j} \frac{d}{dt}\omega_j = T_j - r_{ej}[\cos\delta_j \quad \sin\delta_j] \begin{bmatrix} f_{xj} \\ f_{yj} \end{bmatrix}, \qquad j = 1, \ldots, 4 \quad (2)$$

where $I_{\omega j}$ denotes the inertia for wheel j.

Path-tracking kinematics:

$$\dot{y}_c = -v\sin\phi \quad (3)$$

$$\dot{\phi} = -\frac{v}{y_c}\cos\phi + \dot{\beta} + \gamma. \quad (4)$$

In this paper, we focus on a model obtained via linearizing the vehicle system (1)–(4) around the free-rolling equilibrium point, i.e., $v = v_0$, $\beta = 0$, $\gamma = 0$, $y_c = 0$, and $\phi = 0$, which is described as

$$\dot{x} = Ax + BKu_s + R \quad (5)$$

where $x = [(v - v_0) \quad \beta \quad \gamma \quad y_c \quad \phi]^\perp$ are measurable states, $u_s = [T_1^c + T_1^r \quad T_2^c + T_2^r \quad T_3^c + T_3^r \quad T_4^c + T_4^r \quad \delta_f^c \quad \delta_r^c]^\perp$ are the torques and steering controllers' output vector, T_j^c is used for the path-tracking control design, while T_j^r is applied to overcome the external resistance, which is denoted as $R = [\bar{R} \quad 0 \quad 0 \quad 0 \quad 0]^\perp$. $\bar{R}$ is assumed to be a known constant around the free-rolling equilibrium point. Denote the plant input vector as $\bar{u} = [T_1 \quad T_2 \quad T_3 \quad T_4 \quad \delta_f \quad \delta_r]^\perp$, as shown in Fig. 1. $\bar{u} = Ku_s$, with K defined as the actuator gain matrix, and $K = \mathrm{diag}[\eta_1, \eta_2, \ldots, \eta_6]$, where $\eta_i = 1$ in the healthy situation and will be defined later for the faulty cases. Moreover

$$A = \begin{bmatrix} 0 & 0 & 0 & 0 & 0 \\ 0 & -\frac{C_f + C_r}{mv_0} & -\frac{l_f C_f - l_r C_r}{mv_0^2} - 1 & 0 & 0 \\ 0 & -\frac{l_f C_f - l_r C_r}{J_z} & -\frac{l_f^2 C_f + l_r^2 C_r}{J_z v_0} & 0 & 0 \\ 0 & 0 & 0 & 0 & -v_0 \\ 0 & -\frac{C_f + C_r}{mv_0} & -\frac{l_f C_f - l_r C_r}{mv_0^2} & 0 & 0 \end{bmatrix}$$

$$B = \begin{bmatrix} \frac{1}{mr_{e_1}} & \frac{1}{mr_{e_2}} & \frac{1}{mr_{e_3}} & \frac{1}{mr_{e_4}} & 0 & 0 \\ 0 & 0 & 0 & 0 & \frac{C_f}{mv_0} & \frac{C_r}{mv_0} \\ \frac{-l_d}{J_z r_{e_1}} & \frac{l_d}{J_z r_{e_2}} & \frac{-l_d}{J_z r_{e_3}} & \frac{l_d}{J_z r_{e_4}} & \frac{l_f C_f}{J_z} & -\frac{l_r C_r}{J_z} \\ 0 & 0 & 0 & 0 & 0 & 0 \\ 0 & 0 & 0 & 0 & \frac{C_f}{mv_0} & \frac{C_r}{mv_0} \end{bmatrix}.$$

The constant coefficients C_f and C_r are the cornering stiffness of the front and rear wheels. $C_f = C_{f1} + C_{f2}$, and $C_r = C_{r1} + C_{r2}$. The pair (A, B) is controllable. Note that the developed model is more general than the usual vehicle's lateral model, as in [3] and [5], where only δ_f and δ_r are applied as inputs, and the resistance factors are not considered.

The structure of B ensures the existence of constant torques T_i^r, $i = 1, 2, 3,$ and 4, such that

$$\sum_{i=1}^{4} \left(\frac{\eta_i T_i^r}{mr_{e_i}} \right) = -\bar{R} \quad (6)$$

$$\sum_{i=1}^{4} \left(\frac{(-1)^i l_d \eta_i T_i^r}{J_z r_{e_i}} \right) = 0. \quad (7)$$

Equations (6) and (7) mean that the first row of vector BKu_s equals $-\bar{R}$, and the third row of BKu_s equals 0. This implies that four constant torques T_i^r can be applied to overcome the external resistance.

The input constraints have to be considered for the saturation property of the wheel slip, which is related to the road condition. The relation between input (T_i, δ_i) and the wheel slip S_i at the free-rolling equilibrium point can be given as in [4] and [17]

$$S_i = \begin{bmatrix} \frac{T_i k_i}{r_{ei} C_{fi}} \\ -\beta - \frac{l_f}{v_0}\gamma + \delta_i \end{bmatrix}, \qquad i = 1 \text{ and } 2 \quad (8)$$

$$S_i = \begin{bmatrix} \frac{T_i k_i}{r_{ei} C_{ri}} \\ -\beta - \frac{l_r}{v_0}\gamma + \delta_i \end{bmatrix}, \qquad i = 3 \text{ and } 4 \quad (9)$$

where k_i represents the tire-tread-profile attenuation factor. From (8) and (9), it can be seen that T_i and δ_i need to be constrained to ensure that the magnitude of S_i is below the prescribed value c, i.e., $\|S_i\| \le c$, with $\|\cdot\|$ being the Euclidean norm. More precisely, since $\eta_i T_i^r$ is a constant, a constant bound can be imposed on $\eta_i T_i^c$, while a state-dependent bound should be imposed on $\eta_i \delta_i^c$.

The control objective in the healthy situation is to let the vehicle track the reference path, i.e., make the origin of the system (5) asymptotically stable and, meanwhile, restrict the magnitude of S_i into the prescribed region to prevent the vehicle from skidding or spinning.

B. Fault Setting

Once an actuator fault occurs at $t = t_f$, system (5) can be represented as

$$\dot{x} = Ax + B_f u_s + R \quad (10)$$

where $B_f \triangleq BK$ denotes the fault input distribution matrix. It is assumed that (A, B_f) is still controllable. If (A, B_f) is uncontrollable, then the related faults are said to be unrecoverable by the FTC law; see [14] for more discussions. In this paper, both faults of steering systems and wheel torque control systems are considered. Four faulty cases are investigated:

- F1) The failure of one steering controller (front or rear), which may result from the broken wires, the malfunction power amplifier, or the steeling motor breakdown. In this case, the steering actuator floats with zero moment and does not contribute to the control authority. Consequently, $\eta_5 = 0$, or $\eta_6 = 0$, which is consistent with $B_{f5} = \mathbf{0}$ or $B_{f6} = \mathbf{0}$, where B_{fi} denotes the ith column of B_f.
- F2) The loss of control effectiveness of steering controllers, which does not destroy the steering controller but influences its control gain. In this case, η_5 and η_6 represent the loss of effectiveness factors and are such that $0 < \eta_5 < 1$ and $0 < \eta_6 < 1$. If $\eta_i = 0$, this faulty case is consistent with F1.
- F3) The failure of wheel torque controllers, which may result from the inverter failure, the brake system failure, or the wheel motor failure, such that no torque input is generated. In this case, $\eta_i = 0$, or $B_{fi} = \mathbf{0}$, $i \in \{1, 2, 3, 4\}$.
- F4) The loss of control effectiveness of wheel torque controllers, which does not destroy the torque controller but influences its control gain. Consequently, $0 < \eta_i < 1$, $i \in \{1, 2, 3, 4\}$.

Assumption 1: The vehicle starts around its free-rolling equilibrium point and stays sufficiently close to this equilibrium point in spite of faults. The wheel is running on a regular tire/road condition.

Under Assumption 1, the validity of the linearized model (5) is ensured, and the regular tire/road condition [4] validates the tire model (8) and (9). The FTC objective in this paper is *to let the vehicle track the reference path in spite of input constraints, external resistance, and actuator faults F1–F4.*

III. Fault-Tolerant Control Design

In the sequel, we consider that the torque inputs T_r^j are chosen to overcome the resistance term R, i.e., (6) and (7) are solvable. This implies that at least two-wheel torque controllers are available. Consequently, (5) and (10) are rewritten as

$$\dot{x} = Ax + Bu \tag{11}$$

$$\dot{x} = Ax + B_f u \tag{12}$$

where $u = [T_1^c \quad T_2^c \quad T_3^c \quad T_4^c \quad \delta_f^c \quad \delta_r^c]^\perp$.

We will first recall the PA strategy proposed in [14], analyze its availability in the presence of input constraints, and then combine such optimal FTC approach with the CLF-based bounded controller. The resulting hybrid control approach takes both advantages of the optimal control and the bounded control.

A. LQ-Based PA Control

The LQ optimal control objective is to transfer the system state from the initial value $x(0) = x_0$ to some final value $x(\infty)$, while minimizing the cost function

$$J(u, x_0) = \int_0^\infty (u^\perp R u + x^\perp Q x) dt$$

where Q and R are symmetric matrices. From the classical theory, the solution is given by $u = -R^{-1}B^\perp P_n x \triangleq -F_n x$, where P_n is the unique positive definite solution of the algebraic Riccati equation $P_n A + A^\perp P_n + Q - P_n B R^{-1} B^\perp P_n = 0$.

In practical faulty situations, three time instants, namely, t_f, t_{fdi}, and t_{ftc}, have to be considered, leading to four time windows: $[0, t_f[$: nominal system, (A, B) is controlled by $u = -F_n x$; $[t_f, t_{fdi}[$: diagnostic delay, (A, B_f) is controlled by $u = -F_n x$; $[t_{fdi}, t_{ftc}[$: FTC delay, (A, B_f) is controlled by $u = -F_n x$; and $[t_{ftc}, \infty)$: fault is accommodated, (A, B_f) is controlled by the FTC law.

The pair (A, B) is changed into (A, B_f) at time t_f due to the actuator faults. Once B_f has been identified at $t = t_{fdi}$ under some fault-diagnosis schemes, the classic FTC law can be designed as $u = -R^{-1}B_f^\perp P_f x$ and applied at $t = t_{ftc}$, where P_f is the unique positive definite solution of

$$P_f A + A^\perp P_f + Q - P_f B_f R^{-1} B_f^\perp P_f = 0. \tag{13}$$

The delay $t_{ftc} - t_{fdi}$ is mainly due to the computation of the Riccati equation (13).

The PA strategy aims at minimizing the cost in $t_{ftc} - t_{fdi}$. Such a strategy is based on the following Newton–Raphson scheme.

Let P_i be the unique solution of the Lyapunov equation

$$P_i(A_f - B_f F_{i-1}) + (A_f - B_f F_{i-1})^\perp P_i = -Q - F_{i-1}^\perp R F_{i-1} \tag{14}$$

where $F_i = R^{-1}B_f^\perp P_i$, for all $i = 1, 2, \ldots$, and F_0 is given.

The Newton–Raphson scheme is one of the effective solutions for (13). The computation of (14) is much faster than (13). The PA strategy is to apply $u_i = -F_i x$ as soon as it is obtained. The system behavior after the fault occurrence is therefore

$$\begin{aligned}
\dot{x} &= (A - B_f F_n)x, && t \in [t_f, t_0[\\
\dot{x} &= (A - B_f F_0)x, && t \in [t_0, t_1[\\
\dot{x} &= (A - B_f F_i)x, && t \in [t_i, t_{i+1}[, \qquad i = 1, 2, \ldots
\end{aligned}$$

where $t_0 > t_{fdi}$ and F_0 define the algorithm initialization. It has been proven in [14] that $lim_{i\to\infty} P_i = P_f$, and the PA strategy significantly reduces the loss in cost that results from the classic FTC law in the time delay $t_{ftc} - t_{fdi}$.

Now, we consider the input constraints. In the fault-free situation, $u = -F_n x$ is applied. We can find a region

$$\Psi = \{x \in \Re^n | x^\perp P_n x \le r\} \tag{15}$$

where r is small enough such that, $\forall x \in \Psi$, the ith input $|u_i| < u_i^{\max}(x)$, $\forall i = \{1, \ldots, 6\}$. $u_i^{\max}(x) > 0$ is a constant or a state-dependent bound of the ith input from (8) and (9). It follows that if the initial state $x(0)$ is chosen within Ψ, then $u = -F_n x$ is always available.

In the faulty situation during $[t_i, t_{i+1}[$, the PA control law $u = -F_i x$ is applied. Note that, after the fault occurs, T_i^r is adjusted to overcome R. Denote

$$\Delta\eta_i T_i^r \triangleq \eta_i T_i^r - \eta_{i(n)} T_{i\,(n)}^r$$

where $\eta_{i(n)} T_{i\,(n)}^r$ is related to the fault-free situation, and $\eta_i T_i^r$ corresponds the new controller in the faulty case. If all $\eta_i \neq 0$ $i = 1, 2, 3,$ and 4, then each $\eta_i T_i^r$ keeps a unique constant throughout the process, i.e., $\Delta\eta_i T_i^r = 0$, and does not affect the bound of T_i^c. Similarly, define the region

$$\bar{\Psi}_i = \{x \in \Re^n | x^\perp P_i x \le \varepsilon_i\} \tag{16}$$

where ε_i is small enough such that, $\forall x \in \bar{\Psi}_i$, $|u_i| < u_i^{*\max}(x) \triangleq ((u_i^{\max}(x) - \Delta\eta_i T_i^r)/\eta_i)$, for $\eta_i \neq 0$, and $u_i^{*\max}(x) = 0$, for $\eta_i = 0$,

where $u_i^{\max}(x) - \Delta\eta_i T_i^r$ $(i = 1, 2, 3,$ and $4)$ is assumed to be positive, and T_5^r and T_6^r do not exist. If $\eta_i = 0$, it follows that $u_i = 0$ from the LQ control method. Note that if $x(t_i) \in \bar{\Psi}_i$, then $u = -F_i x$ is available throughout the interval $[t_i, t_{i+1}[$. We also obtain the following property.

Proposition 1: If $x(t_i) \in \bar{\Psi}_i$ such that $\forall j = \{1, \ldots, 6\}$, $\|(-R^{-1}B_f^{\perp})_j\|\|P_i\|\|x\| \le (u_i^{*\max}(x)/\eta_i)$, then the PA strategy is available throughout the interval $[t_i, \infty)$.

Proof: The result follows the fact that the iterating algorithm (14) leads to $P_f \le \cdots \le P_{i+1} \le P_i \le \cdots \le P_1$ [14]. Since $x(t_i) \in \bar{\Psi}_i$, then under the controller $-F_i x$, $\bar{\Psi}_i$ is an invariant set for x, i.e., $x(t) \in \bar{\Psi}_i$, $\forall t \in [t_i, t_{i+1}[$. $\|(-R^{-1}B_f^{\perp})_j\|\|P_1\|\|x\| \le (u_i^{*\max}(x)/\eta_i)$ implies that $\|(-R^{-1}B_f^{\perp})_j\|\|P_{i+1}\|\|x\| \le (u_i^{*\max}(x)/\eta_i)$; thus, $-F_{i+1}x$ is available throughout the interval $[t_{i+1}, t_{i+2}[$, and $\bar{\Psi}_i$ is still an invariant set for x. Finally, it can be concluded that the optimal FTC strategy is available for $t \in [t_i, \infty)$. ■

Such a property is useful for reducing the computation level. If we have checked at $t = t_i$ that $\|(-R^{-1}B_f^{\perp})_j\|\|P_1\|\|x\| \le (u_i^{*\max}(x)/\eta_i)$, then we do not have to check at every following instants t_κ, for $\kappa \ge i$.

However, we cannot always guarantee the availability of the PA strategy. If $x(t_i) \notin \bar{\Psi}_i$, such a strategy would lead to the input saturation, and the system's performance will be degraded.

B. CLF-Based Control

To avoid the input saturation, a CLF-based bounded FTC method is developed, which will be combined with the PA strategy.

Reformulate the faulty system (12) as

$$\dot{x} = Ax + Bu + Bf \tag{17}$$

where the fault is represented as an additive term Bf. $f = (K - I)u$, where I is the unit matrix, and $K = \mathrm{diag}[\eta_1, \ldots, \eta_6]$, with $0 \le \eta_i \le 1$ defined in Section II-B. Since the system inputs are bounded, it is reasonable to assume that actuator faults are bounded, i.e., $\|f\| \le \bar{f}$, where $\bar{f} > 0$. It is also assumed that $\|\Delta\eta_i T_i^r\| \le \bar{\Delta}_i$, for $\bar{\Delta}_i > 0$, and $u_i^{\max}(x) - \bar{\Delta}_i$ $(i = 1, 2, 3, 4)$ is positive.

Consider a Lyapunov function $V = x^{\perp}Px$ for system (17), where P is a positive definite symmetric matrix that satisfies the Riccati equation $A^{\perp}P + PA - PBB^{\perp}P = -W$ for a positive definite matrix W.

V can be regarded as a CLF for system (17). The bounded FTC law is designed as

$$u_i = -K_i(V)(L_{B_i}V)^{\perp}(x) \triangleq b_i(x), \qquad i = 1, \ldots, 6 \tag{18}$$

with

$$K_i(V) = \frac{\vartheta(V) + \sqrt{\vartheta(V)^2 + \left(u_i^{\star\max}(x)\,\|(L_{B_i}V)^{\perp}\|\right)^4}}{\|(L_{B_i}V)^{\perp}\|^2\left[1 + \sqrt{1 + \left(u_i^{\star\max}(x)\,\|(L_{B_i}V)^{\perp}\|\right)^2}\right]}$$

for $(L_{B_i}V)^{\perp} \ne 0$, and $K_i(V) = 0$, for $(L_{B_i}V)^{\perp} = 0$, where $\vartheta(V) \triangleq (1/6)(L_{Ax}V + \rho V + \|L_I V\|\bar{f})$, L denotes the Lie derivative, i.e., $L_{Ax}V = x^{\perp}(A^{\perp}P + PA)x$, $(L_{B_i}V)^{\perp} = 2B_i^{\perp}Px$, and $\rho > 0$. $u_i^{\star\max} \triangleq u_i^{\max}(x) - \bar{\Delta}_i$.

For all initial states, the stability region of system (17) is defined by the set

$$\Omega = \{x \in \Re^n | V(x) \le c^{\max}\} \tag{19}$$

where $c^{\max}$ is small enough such that $\vartheta(V) < \min_{i\in\{1,2,\ldots,6\}} u_i^{\star\max}(x)\|(L_{B_i}V)^{\perp}(x)\|$ for all $x \in \Omega$.

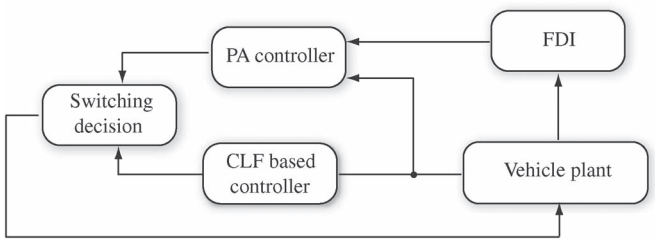

Fig. 2. Block diagram of the FTC system.

Proposition 2: For the initial state $x(0) \in \Omega$, the bounded controller $u = b(x)$, with $b(x) \triangleq [b_1(x), \ldots, b_6(x)]^{\perp}$ in (18), makes the origin of system (17) asymptotically stable in spite of faults.

Proof (sketch): Based on the derivative of V along the closed-loop trajectories, it can be obtained that, whenever $\vartheta(V) < u_i^{\star\max}(x)\|(L_{B_i}V)^{\perp}(x)\|$, we have $\dot{V} < -\rho V$. Thus, starting from any initial state $x(0) \in \Omega$, $\dot{V} < -\rho V$, the state cannot escape the region Ω, and the origin of the system is asymptotically stable. ■

Proposition 2 provides a result for the multiple-state-dependent input constraint form, i.e., $|u_i| < u_i^{\star\max}(x)$, $i = 1, \ldots, 6$, which is more general than the form $\|u\| < u^{\max}$ in [16]. It can be seen that, for any $x(0) \in \Omega$, the controller $u = b(x)$ can always be applied and does not need to be modified in the presence of faults.

C. Hybrid Control Approach

Based on the analysis in Sections III-A and B, a hybrid control method can be provided as

$$u = \begin{cases} -F_n x, & \text{for } x \in \Psi \cap \Omega, \quad t \in [0, t_{fdi}[\\ b(x), & \text{for } x \in \Psi \cap \Omega, \quad t \in [t_{fdi}, t_1[\\ -F_i x, & \text{for } x \in \bar{\Psi}_i \cap \Omega, \quad t \in [t_i, t_{i+1}[\\ b(x), & \text{for } x \notin \bar{\Psi}_i \cap \Omega, \quad t \in [t_i, t_{i+1}[\end{cases} \qquad i = 1, 2, \ldots \tag{20}$$

where Ψ, $\bar{\Psi}_i$, and Ω are defined, respectively, in (15), (16), and (19). Fig. 2 shows the block diagram of the control system.

Discussion:

- D1) Compared with the convex conjugacy technique [18] that requires $x \in \Psi$, the bounded hybrid controller (20) restricts x into a relatively small region $\Psi \cap \Omega$, which, however, leads to a low computation level. Since $b(x)$ can be designed offline, we do not have to solve the backward Hamiltonian system every time when x reaches the bound of $\Psi \cap \Omega$, as in [18].
- D2) Since the initial state $x(0) \in \Psi \cap \Omega$, the controller $-F_n x$ ensures that $x(t_f) \in \Psi \cap \Omega$. Nothing can be said about the state trajectory during the diagnosis delay $t_{fdi} - t_f$. Effective diagnosis approaches can significantly shorten this delay. Assuming that $x(t_{fdi})$, $In\Psi \cap \Omega$ is quite acceptable in the practical application.
- D3) Applying $b(x)$ at the beginning of the FTC process $[t_{fdi}, t_1[$ shortens the initial time of the PA strategy in [14]. Moreover, in each interval $[t_i, t_{i+1}[$, once $x \notin \bar{\Psi}_i \cap \Omega$, the controller $b(x)$ can always make x return to $\bar{\Psi}_i \cap \Omega$, as in Proposition 2, such that the controller $-F_i x$ is available.
- D4) The region Ω in (19) is based on a fixed norm bound of faults $\bar{f}$. This region could be zoomed in since faults impossibly exist all the time. See the related work in [16].
- D5) In this paper, a straight reference path is considered, i.e., the curvature $\rho_{ref} \approx 0$. For the curving path with $\rho_{ref} \ne 0$, an additional term $[0 \quad 0 \quad 0 \quad -v_0\rho_{ref}]^{\perp}$ should be added in

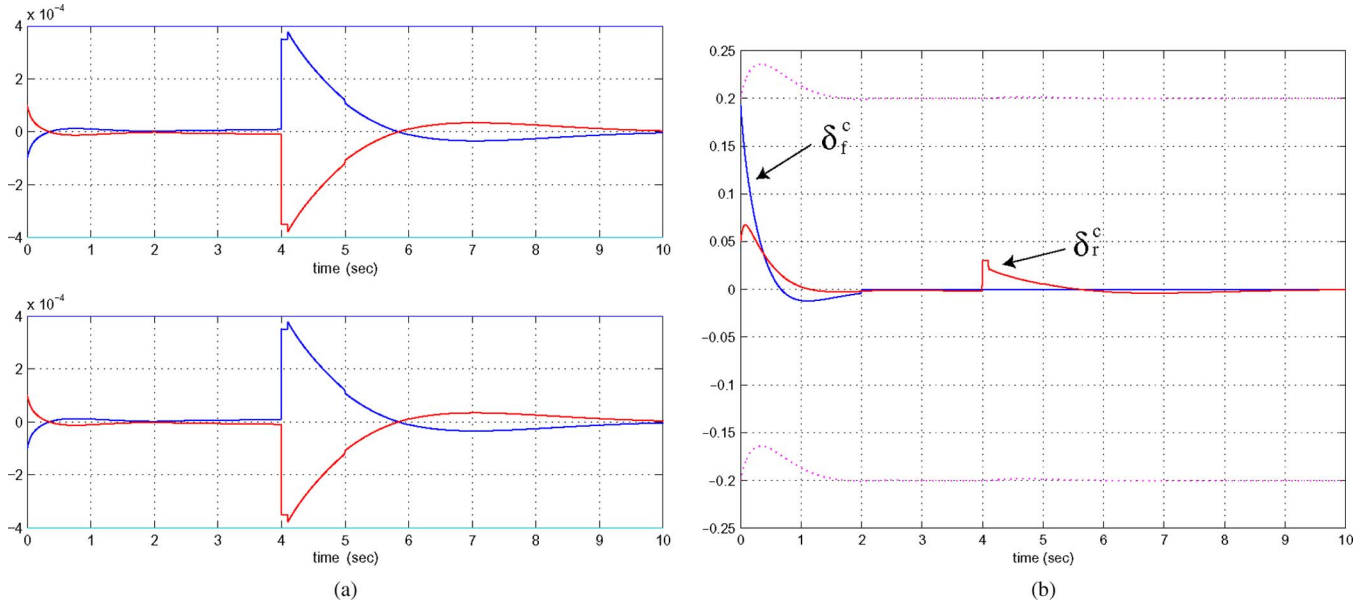

Fig. 3. Input trajectories. (a) Torque inputs. (b) Steering angle inputs.

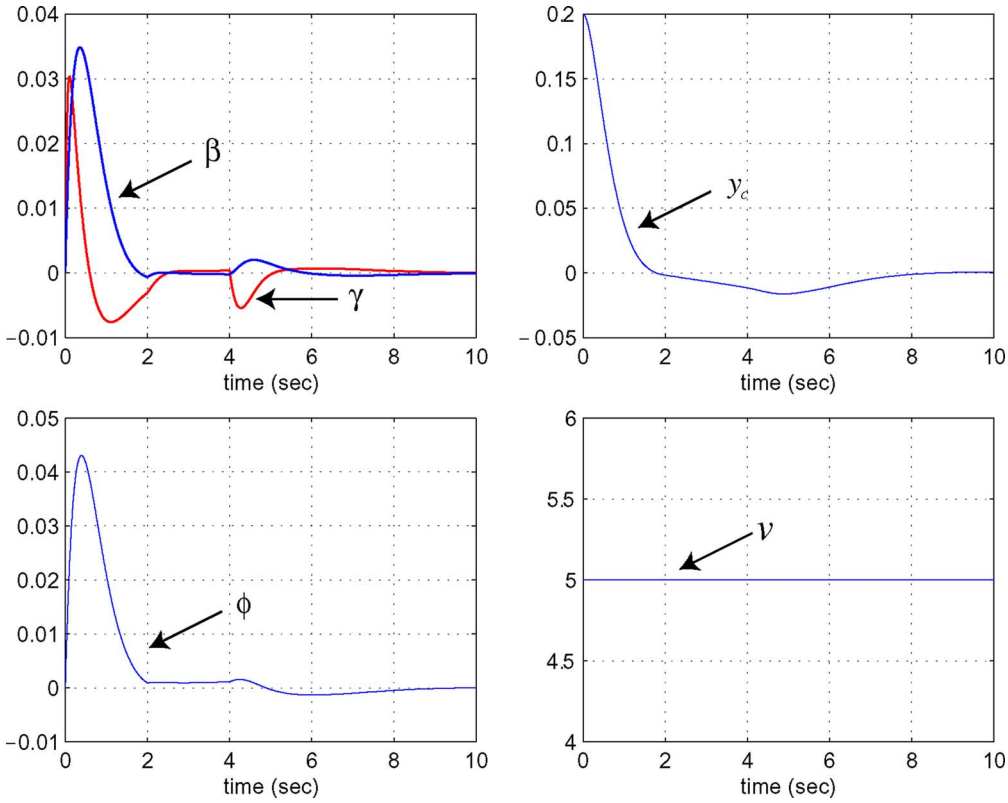

Fig. 4. Vehicle motion behavior.

the system equation (5). The robust design of LQ control [15] and CLF-based control [16] can be applied.

D6) If three-wheel torque controllers are faulty (F3), the remaining wheel torque cannot overcome the resistance factor. This also leads to the robust problem as in D5.

IV. Simulation Results

The proposed method in Section III is now applied to the path tracking of the RobuCar vehicle (5). The parameters are given as $m = 350$ kg, $l_f = 0.401$ m, $l_r = 0.802$ m, $l_d = 0.605$ m, $r_{ei} = 0.350$ m, $C_f = C_r = 2000$ N/rad, $J_z = 82$ kgs^2, and $v_0 = 5$ m/s. The vehicle starts the path tracking with the initial values $v(0) = 5$ m/s, $\beta(0) = 0$ rad, $\gamma(0) = 0$ rad/s, $y_c(0) = 0.2$ m, and $\phi(0) = 0$ rad. The resistance factor $\bar{R}$ is assumed to be -0.5 m/s^2. We set the wheel slip constraint as $c = 0.3$, and the attenuation factor in (8) and (9) is $k_i = 0.2$. The input constraints are imposed as -0.0004 Nm $\leq T_i^c \leq 0.0004$ Nm and $(-0.18+0.08\gamma+\beta)$ rad $\leq \delta_i^c \leq (0.18+0.08\gamma+\beta)$ rad, for $i = 1, \ldots, 4$. Since v is around a constant v_0, small torques T_i^c are required.

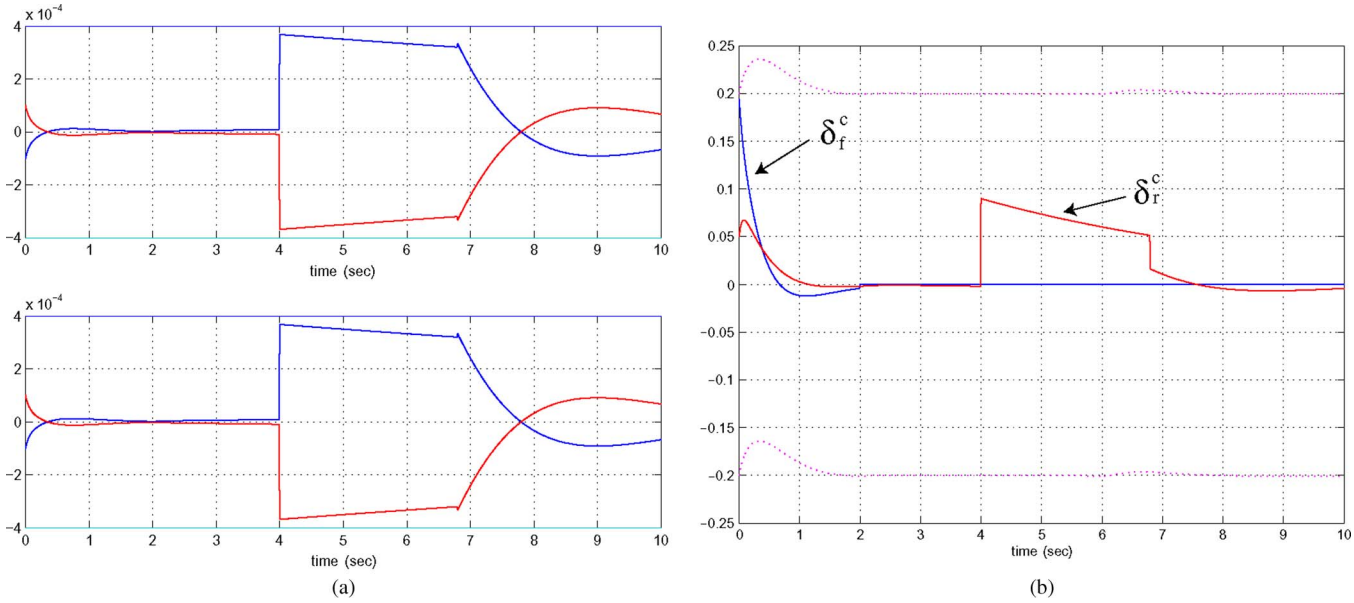

Fig. 5. Input trajectories. (a) Torque inputs (b) Steering angle inputs.

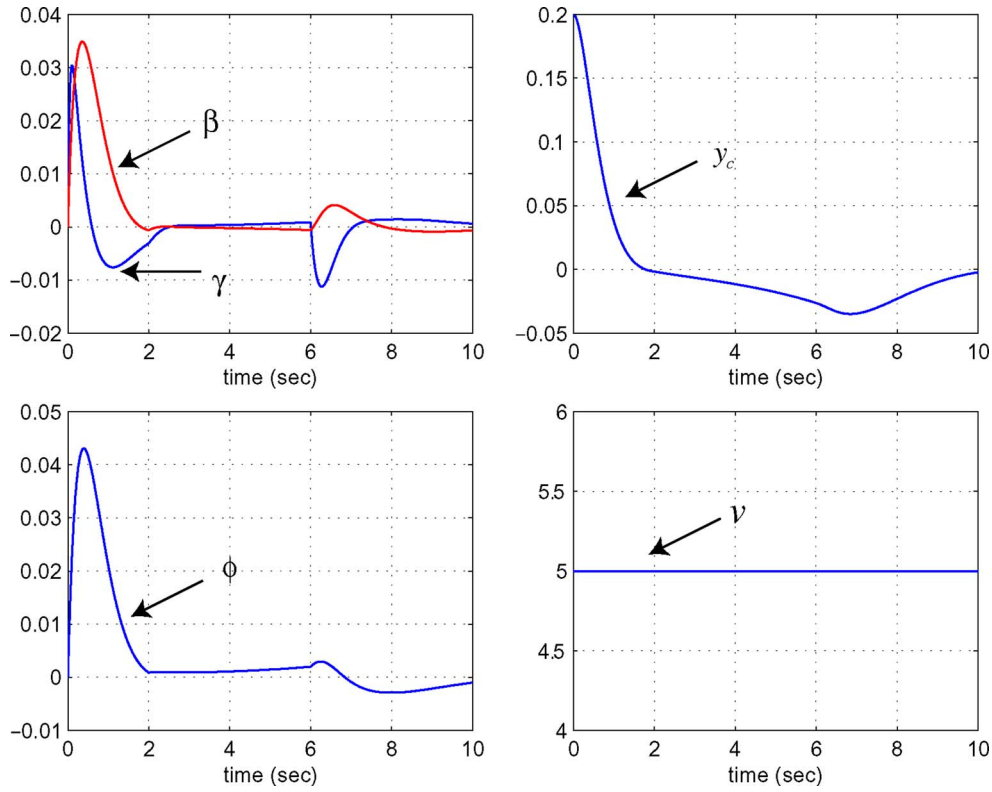

Fig. 6. Vehicle motion behavior.

The objective is to obtain the tracking behavior in spite of faults and input constraints. Due to limited space, we will only consider F1 and F2 described in Section II-B.

Suppose that the front steering system is broken at $t = 2$ s, which leads to $\eta_1 = 0$. Such failure is also consistently represented by $B_{f5} = \mathbf{0}$. In addition, there is a 90% loss of control effectiveness in the power amplifier of the rear-steering actuator after $t = 2$ s, i.e., $\eta_6 = 0.1$. In this case, the tracking performance is maintained only by applying T_1, T_2, T_3, T_4, and δ_r.

Choose $W = Q = \mathrm{diag}[1, 1, 1, 1]$. The classic FTC law $u_f = -F_f x$ can be obtained after three iterations of (14), i.e., $F_f = F_3$. To illustrate our approach, assume that it takes 2 s for fault diagnosis, 0.1 s for the initialization of the PA strategy, and 0.9 s for each iteration of PA. However, $-F_1 x$ exceeds the input bound of T_i at $t = 4.1$ s; thus, the CLF-based controller is applied until 4.2 s, and then, the PA controller is activated. $-F_2 x$ satisfies the property of Proposition 1 at $t = 5$ s, which implies that the PA control is always available after 5 s.

Fig. 3 shows the trajectories of the hybrid controller. It can be seen that all T_i^c and δ_r^c are abruptly adjusted to compensate for the faults. All the torques $T_i^r = 15.315$ Nm, $i = 1, 2, 3,$ and 4, which do not change since no fault occurs at the torque control system. Fig. 4

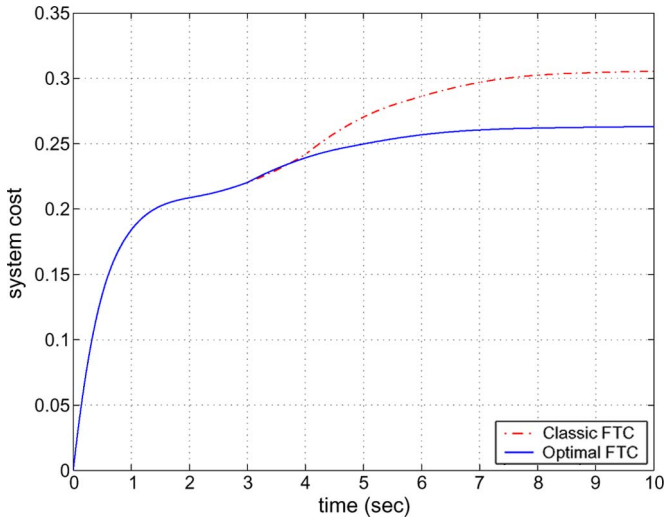

Fig. 7. Cost comparison.

illustrates the vehicle motion behavior. After $t = 2$ s, the trajectory of the vehicle deviates from the reference path, while the tracking goal is achieved at nearly $t = 8$ s, and v is always maintained at 5 m/s.

Fig. 5 illustrates the trajectories of the controller that combines the classic LQ method and the CLF technique. The classic LQ controller exceeds the constraints at $t = 5.9$ s and is not applied until $t = 6.8$ s. It can be seen that much more control effort has to be made than the hybrid control one. Fig. 6 illustrates the vehicle motion behavior. The vehicle again tracks the path at nearly $t = 10$ s.

Fig. 7 gives the evolution of the system cost with the classic and PA methods, which implies the good system performance under the proposed hybrid approach.

V. Conclusion

This paper has proposed an optimal hybrid FTC approach with application to the path-tracking control problem for the 4WS4WD RobuCar vehicle at LAGIS. Several important types of actuator faults have been addressed. Future work will concern robust fault-tolerant path-tracking control design of 4WS4WD vehicles.

References

[1] C. C. Chan, "The state of the art of electric, hybrid, and fuel cell vehicles," *Proc. IEEE*, vol. 95, no. 4, pp. 704–718, Apr. 2007.
[2] X. He and J. W. Hodgson, "Modeling and simulation for hybrid electric vehicles. I. Modeling," *IEEE Trans. Intell. Transp. Syst.*, vol. 3, no. 4, pp. 235–243, Dec. 2002.
[3] S. Sakai, H. Sado, and Y. Hori, "Motion control in an electric vehicle with four independently driven in-wheel motors," *IEEE/ASME Trans. Mechatron.*, vol. 4, no. 1, pp. 9–16, Mar. 1999.
[4] S. T. Peng, "On one approach to constraining the combined wheel slip in the autonomous control of a 4WS4WD vehicle," *IEEE Trans. Control Syst. Technol.*, vol. 15, no. 1, pp. 168–175, Jan. 2007.
[5] K. Moriwaki, "Autonomous steering control for electric vehicles using nonlinear state feedback H_∞ control," *Nonlinear Anal.*, vol. 63, no. 5–7, pp. e2 257–e2 268, Nov./Dec. 2005.
[6] I. Unger and R. Isermann, "Fault tolerant sensors for vehicle dynamics control," in *Proc. Amer. Control Conf.*, Minneapolis, MN, 2006, pp. 3948–3953.
[7] S. C. Subramanian, S. Darbha, and K. R. Rajagopal, "A diagnostic system for air brakes in commercial vehicles," *IEEE Trans. Intell. Transp. Syst.*, vol. 7, no. 3, pp. 360–376, Sep. 2006.
[8] Z. Gao, S. X. Ding, and Y. Ma, "Robust fault estimation for vehicle lateral dynamic systems," in *Proc. IFAC SAFEPROCESS*, Beijing, China, 2006, pp. 1039–1043.
[9] R. Rajamani, A. S. Howell, C. Chieh, J. K. Hedrick, and M. Tomizuka, "A complete fault diagnostic system for automated vehicles operating in a platoon," *IEEE Trans. Control Syst. Technol.*, vol. 9, no. 4, pp. 553–564, Jul. 2001.
[10] P. E. Dumont, A. Aïtouche, and M. Bayart, "Fault detection of actuator faults for electric vehicle," in *Proc. 16th IEEE Int. Conf. Control Appl.*, Mumbai, India, 2007, pp. 1067–1072.
[11] M. Blanke and J. S. Thomsen, "Electrical steering of vehicles—Fault tolerant analysis and design," *Microelectron. Reliab.*, vol. 46, no. 9–11, pp. 1421–1432, Sep.–Nov. 2006.
[12] P. E. Dumont, A. Aïtouche, R. Merzouki, and M. Bayart, "Fault tolerant control on an electric vehicle," in *Proc. Int. Conf. Ind. Technol.*, Singapore, 2006, pp. 2450–2455.
[13] [Online]. Available: http://www.robosoft.fr/eng/
[14] M. Staroswiecki, H. Yang, and B. Jiang, "Progressive accommodation of parametric faults in linear quadratic control," *Automatica*, vol. 43, no. 12, pp. 2070–2076, Dec. 2007.
[15] M. Staroswiecki, "Robust fault tolerant linear quadratic control based on admissible model matching," in *Proc. 45th IEEE Conf. Decision Control*, 2006, pp. 3506–3511.
[16] H. Yang, B. Jiang, and V. Cocquempot, "Observer-based fault tolerant control for constraint switched systems," *Int. J. Control Autom. Syst.*, vol. 5, no. 6, pp. 707–711, 2007.
[17] J. Ackermann, *Robust Control*. London, U.K.: Springer-Verlag, 1993.
[18] R. Goebel and M. Subbotin, "Continuous time linear quadratic regulator with control constraints via convex duality," *IEEE Trans. Autom. Control*, vol. 52, no. 5, pp. 886–892, May 2007.

Controller for Urban Intersections Based on Wireless Communications and Fuzzy Logic

Vicente Milanés, Joshué Pérez, Enrique Onieva, and Carlos González, *Member, IEEE*

***Abstract*—A major research topic in intelligent transportation systems (ITSs) is the development of systems that will be capable of controlling the flow of vehicular traffic through crossroads, particularly in urban environments. This could significantly reduce traffic jams, since autonomous vehicles would be capable of calculating the optimal speed to maximize the number of cars driving through the intersection. We describe the use of vehicle-to-vehicle (V2V) communications to determine the position and speed of the vehicles in an environment around a crossroad. These data are used to estimate the intersection point, and a fuzzy controller then modifies the speed of the cars without right of way according to the speed of the car with right of way. Experimental tests conducted with two mass-produced cars on a real circuit at the facilities of the Instituto de Automática Industrial, Consejo Superior de Investigaciones Científicas, Madrid, Spain, gave excellent results.**

***Index Terms*—Accident detection, autonomous vehicles, fuzzy control, intervehicle communication, traffic management.**

Manuscript received March 26, 2009; revised July 6, 2009. First published December 1, 2009; current version published March 3, 2010. This work was supported in part by Plan Nacional, Spain, under Project TRANSITO under TRA2008-06602-C03-01, by the Comisión Interministerial de Ciencia y Tecnología, Spain, under Project GUIADE (Spain Ministerio de Fomento T9/08), and by the National Strategic Consortia for Technical Research (CENIT) under Project MARTA (CENIT-20072006). The Associate Editor for this paper was Prof. U. Nunes.

The authors are with the Industrial Computer Science Department, Instituto de Automática Industrial, Consejo Superior de Investigaciones Científicas, 28500 Madrid, Spain (e-mail: vmilanes@iai.csic.es; jperez@iai.csic.es; onieva@iai.csic.es; gonzalez@iai.csic.es).

Color versions of one or more of the figures in this paper are available online at http://ieeexplore.ieee.org.

Digital Object Identifier 10.1109/TITS.2009.2036595